GSA Data Repository for:
S.E.K. Bennett et al., Transtensional rifting in the proto–Gulf of California near Bahía Kino, Sonora, México: *GSA Bulletin*, doi: 10.1130/B30676.1.

SUPPLEMENTAL MATERIAL

FAULT KINEMATICS

Methods

Structural observations and fault kinematic data were collected from fault planes in outcrop (e.g. Fig. 4H, I) where fault-slip indicators (slickenlines or mullions) were preserved (e.g. Fig. 4J, K). 132 fault-slip indicators were measured within all non-Quaternary map units. Each fault-slip measurement consists of the strike/dip of the fault plane, rake of fault slip indicator, and sense of shear. A reliable shear sense indicator was absent for ~80% of the measured striae. Thus, a shear sense direction was systematically assigned to each fault kinematic datum based on models of predictable transtensional structures (e.g. Withjack and Jamison, 1986) formed from dextral oblique extension (e.g. a west-dipping fault with dip-slip slickenlines is assigned an extensional, not compressional, shear-sense indicator).

Analysis

For this kinematic analysis, slickenlines are assumed to form in the direction of the maximum resolved shear stress on a fault plane (Wallace, 1951; Bott, 1959). Thus, the paleo-directions of the most compressive and least compressive principal stresses on that fault form components of the orientation of the fault slickenline or mullion datum. Together these data, in the context of the orientation of the fault plane on which they are measured, yield a set of principal strain directions. If these represent infinitesimal strain (i.e. small-offset faults that have not been subsequently rotated) the strain axes should be representative of paleo-stress principal axes. Principal paleo-stress axes were determined using FaultKin v.4.3.5 software (Marrett and Allmendinger, 1990; Allmendinger et al., 2012), which utilizes the right dihedra geometrical method of Angelier and Mechler (1977) and Pfiffner and Burkhard (1987).

Variable amounts of clockwise vertical-axis rotation of fault blocks have occurred across the study area. This rotation greatly complicates the analysis, as faults may have slipped at an orientation different than that measured in outcrop. In our analysis we assume that the faults measured were formed prior to rotation. All fault kinematic data were thus rotated counter-clockwise about a vertical-axis by the amount of rotation either determined by the paleomagnetic results of this study (up to 53°), or predicted from strain compatibility with adjacent blocks.

Results

Fault kinematic data are highly variable and do not show a consistent relationship between fault dip and rake or fault strike and rake (Fig. DR1). This suggests that many faults have been rotated since their formation, complicating kinematic analysis. Overall the fault kinematic data are consistent with transtensional deformation of the area. Fault kinematic indicators measured in pre-12.5 Ma rocks (Fig. DR2A; n=89) are generally ignored in this analysis as they may record older, pre-rift episodes of deformation. Fault kinematic indicators measured in 12.5 - 0 Ma rocks (n=43) reflect all Gulf of California deformation, and display WSW-directed slightly oblique extension (T-axis azimuth 254°) with a near-vertical $\sigma 1$ principal stress (Fig. DR2B).

To test for a change in paleo-stress orientation with time (cf. Angelier et al., 1981), the well-dated stratigraphy was used as a chronologic filter as various periods of time were compared for similar or dissimilar paleo-stress axis orientations. Fault kinematic indicators (n=20) measured in early proto-Gulf rocks (12.5 to 11.5 Ma), which integrate all subsequent Gulf deformation, display a SW-NE slightly oblique extension direction (T-axis azimuth 232°) with a near-vertical $\sigma 1$ principal stress (Fig. DR2C). In latest proto-Gulf rocks (7 to ~6 Ma), fault kinematic indicators (n=23) suggest an approximate E-W slightly oblique extension direction (T-axis azimuth 263°), again with a near-vertical σ1 principal stress (Fig. DR2D). Although the paleo-stress results from the fault kinematic dataset appear to distinguish two distinctly different extension (i.e. σ3 principal stress) directions for early proto-Gulf and latest proto-Gulf time periods, the confidence of this distinction is not high. Confidence contours for P- and T-axes strongly overlap (Fig. DR2). A major limitation of this dataset is that rocks deposited during a large portion of proto-Gulf time (~11.5–7 Ma) are not observed. Therefore, the kinematic data do not represent the tectonic style during a large portion of proto-Gulf time, and overall, these results should be taken with some level of reservation.

REFERENCES CITED

Allmendinger, R.W., Cardozo, N.C., and Fisher, D., 2012, Structural Geology Algorithms: Vectors & Tensors: Cambridge, England, Cambridge University Press, 289 p.

Angelier, J., and Mechler, P., 1977, Sur une méthode graphique de recherche des contraintes principales également utilisable en tectonique et en séismologie: La méthode des dièdres droits: Bulletin de la Société Géologique de France, v. 7, p. 1309–1318.

Angelier, J., Colletta, B., Chorowicz, J., Ortlieb, L., and Rangin, C., 1981, Fault tectonics of the Baja California Peninsula and the opening of the Sea of Cortez, Mexico: Journal of Structural Geology, v. 3, no. 4, p. 347–357, doi:10.1016/0191-8141(81)90035-3.

Bott, M.H.P., 1959, The mechanics of oblique slip faulting: Geological Magazine, v. 96, p. 109–117.

Marrett, R.A., and Allmendinger, R.W., 1990, Kinematic analysis of fault-slip data: Journal of Structural Geology, v. 12, p. 973–986.

Pfiffner, O.A., and Burkhard, M., 1987, Determination of paleostress axes orientations from fault, twin and earthquake data: Annales Tectonicae, v. 1, p. 48–57.

Wallace, R.E., 1951, Geometry of shearing stress and relation to faulting: Journal of Geology, v. 59, p. 118–130.

Withjack, M.O., and Jamison, W.R., 1986, Deformation produced by oblique rifting: Tectonophysics, v. 126, p. 99–124, doi:10.1016/0040-1951(86)90222-2.

FIGURE DR1. (A) Fault Dip vs. Rake for all measured fault striae. (B) Fault Strike vs. Rake for all measured fault striae. See Table DR1 for a list of all measured fault striae.

FIGURE DR2. Fault kinematic data of slickenlines and mullions observed in coastal Sonora study area. Columns display (left) measured faults and striae, (left-center) P-axes (gray circles) and T-axes (black squares) for individual fault measurements, (right-center) Kamb contour of P-axes (gray) and T-axes (black), and (right) fault plane solution. All analysis conducted with FaultKin software (Marrett and Allmendinger, 1990; Allmendinger et al., 2012). (A) Kinematic data from pre-12.5 Ma rocks. (B) Kinematic data from rift-related (post-12.5 Ma) rocks. These rift-related fault data are further subdivided into faults measured in early proto-Gulf-age rocks (C) and in latest proto-Gulf-age rocks (D). It is assumed that the faults formed prior to rotation, which may be invalid. All fault kinematic data plotted here were first rotated counter-clockwise about a vertical-axis by the amount of rotation either determined by the paleomagnetic results of this study (up to 53°).

FIGURE DR1

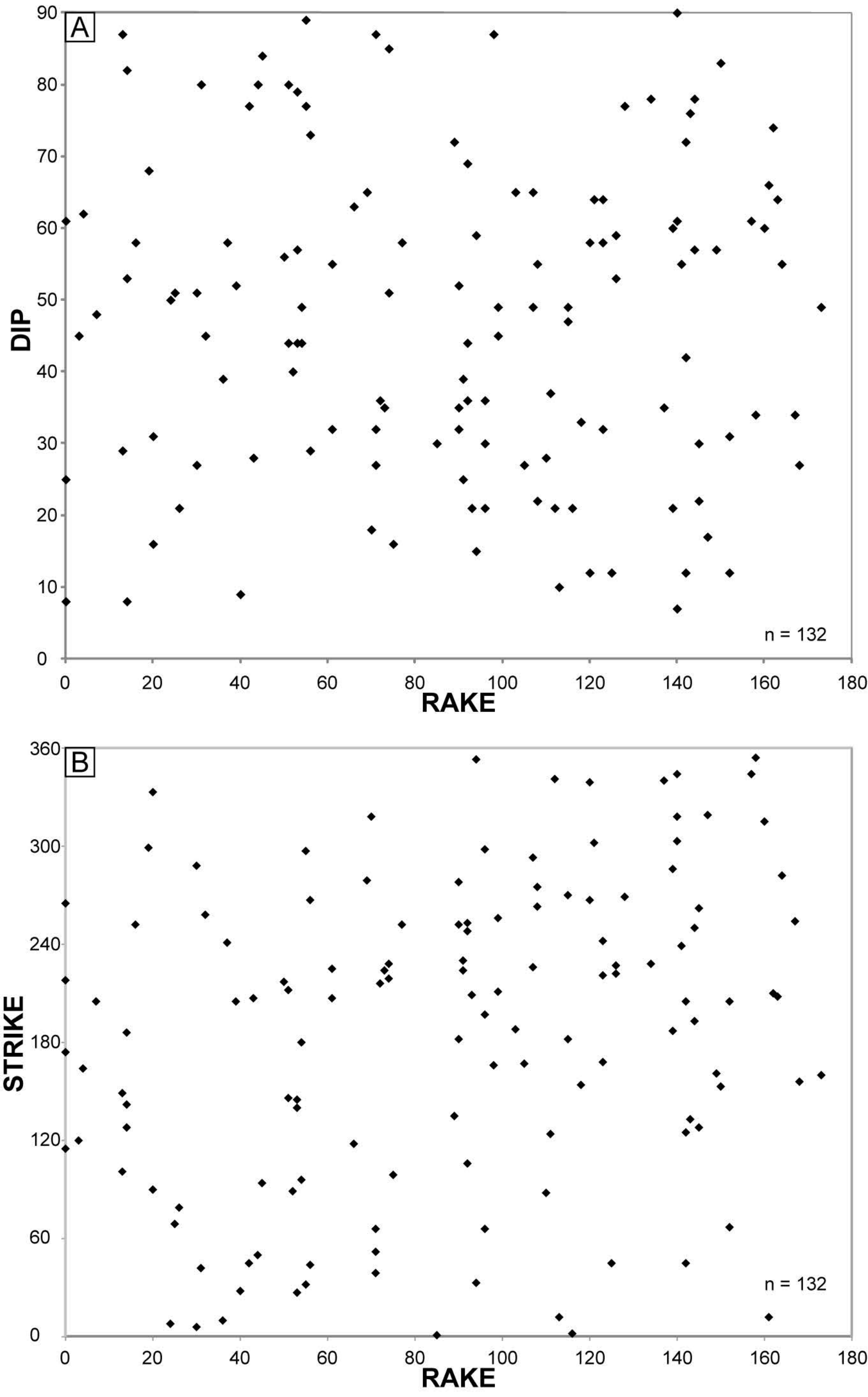

FIGURE DR2

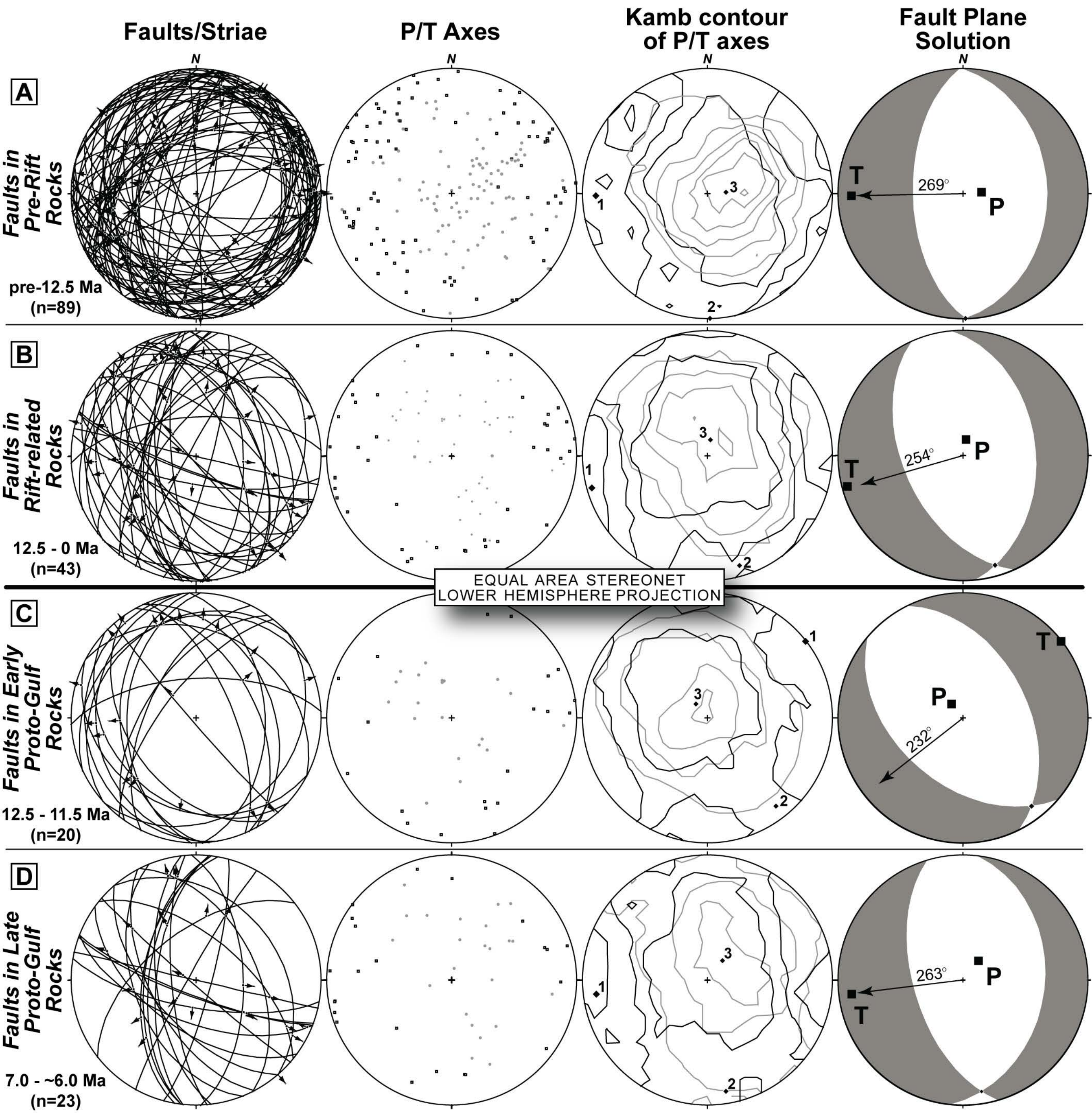
Faults/Striae
P/T Axes
Kamb contour of P/T axes
Fault Plane Solution
N
A
Faults in Pre-Rift Rocks
pre-12.5 Ma
(n=89)
269°
B
Faults in Rift-related Rocks
12.5 - 0 Ma
(n=43)
254°
EQUAL AREA STEREONET
LOWER HEMISPHERE PROJECTION
C
Faults in Early Proto-Gulf Rocks
12.5 - 11.5 Ma
(n=20)
232°
D
Faults in Late Proto-Gulf Rocks
7.0 - ~6.0 Ma
(n=23)
263°
T
P

TABLE DR1. Fault kinematic data measured in the study area.

Map Unit	Strike	Dip	Rake	Sense of Slip	Map Unit	Strike	Dip	Rake	Sense of Slip
Tcu	050	80	44	ND	Tvu	341	21	112	ND
Tcu	164	62	4	dextral	Tvu	115	25	0	ND
Tcu	208	64	163	ND	Tvu	090	16	20	ND
Tcu	222	59	126	ND	Tvu	052	87	71	ND
Tcu	221	64	123	ND	Tvu	340	35	137	ND
Tcu	211	49	99	normal	Tvu	002	21	116	ND
Tcu	166	87	98	ND	Tvu	205	48	7	ND
Tcu	187	60	139	ND	Tvu	193	78	144	ND
Tcu	174	61	0	ND	Tvu	254	34	167	ND
Tcu	217	56	50	normal	Tvu	265	8	0	ND
Tcu	145	79	53	ND	Tvu	315	60	160	ND
Tcu	033	59	94	ND	Tvu	182	32	90	ND
Tcu	161	57	149	ND	Tvu	066	30	96	ND
Tcu	008	50	24	ND	Tvu	167	27	105	ND
Tcu	225	55	61	ND	Tvu	099	16	75	ND
Tcu	210	74	162	ND	Tvu	303	61	140	ND
Tcu	146	80	51	ND	Tvu	293	49	107	ND
Tcu	344	61	157	ND	Tvu	042	80	31	ND
Tcu	135	72	89	ND	Tvu	154	33	118	ND
Tcu	318	90	140	ND	Tvu	252	35	90	ND
Tcu	354	34	158	ND	Tvu	262	22	145	ND
Ttmc	219	85	74	ND	Tvu	226	65	107	ND
Ttsf	302	64	121	normal/dextral	Tvu	228	78	134	ND
Ttsf	010	39	36	ND	Tvu	120	45	3	ND
Ttsf	333	31	20	ND	Tvu	096	49	54	ND
Ttsf	241	58	37	ND	Tvu	224	35	73	normal/sinistral
Ttsf	250	57	144	ND	Tvu	207	32	61	normal/sinitral
Ttsf	149	87	13	ND	Tvu	339	12	120	normal/dextral
Ttsf	079	21	26	ND	Tvu	001	30	85	ND
Ttsf	168	32	123	ND	Tvu	319	17	147	ND
Ttsf	156	27	168	ND	Tvu	227	53	126	ND
Ttsf	209	21	93	ND	Tvu	353	15	94	ND
Ttsf	205	12	152	ND	Tvu	133	76	143	ND
Ttsf	253	69	92	normal	Tvu	067	31	152	ND
Ttsf	6	51	30	ND	Tvu	069	51	25	ND
Ttsf	212	44	51	ND	Tvu	242	58	123	ND
Ttsf	012	66	161	ND	Tvu	128	53	14	ND
Tvln	27	44	53	normal	Tvu	066	27	71	ND
Tvls	180	44	54	ND	Tvu	248	44	92	ND
Tvls	263	22	108	ND	Tvu	282	55	164	ND
Tvls	298	21	96	ND	Tvu	318	18	70	ND
Tvls	230	39	91	ND	Kg	228	51	74	normal
Tvs	088	28	110	ND	Kg	299	68	19	ND
Tvs	270	49	115	ND	Kg	94	84	45	normal
Tvs	267	58	120	ND	Kg	153	83	150	ND
Tvs	239	55	141	ND	Kt dike	045	77	42	ND
Tvs	258	45	32	ND	Kt dike	205	72	142	ND
Tvu	32	89	55	ND	Kt	279	65	69	normal
Tvu	297	77	55	ND	Kt	106	36	92	normal
Tvu	142	8	14	ND	Kt	101	29	13	dextral
Tvu	288	27	30	ND	Kt	118	63	66	ND
Tvu	344	7	140	ND	Kt	218	25	0	sinistral
Tvu	028	9	40	ND	Kt	216	36	72	normal
Tvu	045	12	125	ND	Kt	140	57	53	thrust?
Tvu	045	12	142	ND	Kt	286	21	139	normal
Tvu	188	65	103	ND	Kt	160	49	173	dextral
Tvu	089	40	52	ND	Kt	205	52	39	normal
Tvu	039	32	71	ND	Kt	128	30	145	normal
Tvu	044	29	56	ND	Kt	124	37	111	normal
Tvu	125	42	142	ND	Kt	256	45	99	normal
Tvu	252	58	77	ND	Kt	267	73	56	normal
Tvu	252	58	16	ND	Kt	182	47	115	ND
Tvu	012	10	113	ND	Kt	224	25	91	ND
Tvu	269	77	128	normal/dextral	Kt	186	82	14	ND
Tvu	275	55	108	ND	Kt	207	28	43	ND
Tvu	278	52	90	ND	Pziu	197	36	96	ND

'ND' indicates a fault striae measurment where the sense of fault slip motion was not determinable.